Chitosan Membrane Embedded With ZnO/CuO Nanocomposites for the Photodegradation of Fast Green Dye Under Artificial and Solar Irradiation

Analytical Chemistry Insights
Volume 13: 1–13
© The Author(s) 2018
Reprints and permissions:
sagepub.co.uk/journalsPermissions.nav
DOI: 10.1177/1177390118763361

Eman Alzahrani

Chemistry Department, Faculty of Science, Taif University, Taif, Kingdom of Saudi Arabia.

ABSTRACT: Fast Green (FCF) dye is commonly used in both cytology and histology applications. Previous studies have found that it can cause mutagenic and tumorigenic effects in experimental human and animal populations. It can also be a source of skin, eye, respiratory, and digestive irritation. The purpose of this study was to examine the use of thin film membranes to degrade FCF. A thin film membrane of chitosan (CS) was fabricated and subsequently filled with zinc oxide nanoparticles (ZnO) or ZnO/CuO-heterostructured nanocomposites. The CS membrane was used as a matrix, and the nanomaterials were used as photocatalysts. The prepared membranes were characterised by four analytical techniques: atomic force microscopy, scanning electron microscopy, X-ray diffraction, and energy-dispersive X-ray analyses. The photocatalytic activity of the fabricated membranes was evaluated by performing experiments in which aqueous solutions of FCF dye that contained the fabricated membrane were irradiated with solar light or UV light. The photodegradation percentage was spectrophotometrically determined by monitoring the maximum wavelengths (λ_{max}) of FCF at 623 nm for different irradiation times. The decolourisation percentages of the dye under solar light were 57.90% and 60.23% using the CS-ZnO and CS-ZnO/CuO membranes, respectively. When UV light irradiation was employed as the source of irradiation, the photodegradation percentages of FCF were 71.45% and 91.21% using the CS-ZnO and CS-ZnO/CuO membranes, respectively. These results indicated that the best photocatalytic system for the degradation of FCF dye was CS-ZnO/CuO membrane in combination with UV light irradiation. The study also found that it was easy to separate the prepared membranes after the reaction without the need for a centrifuge or magnet. The results demonstrate the potential for CS-ZnO and CS-ZnO/CuO membranes for use as effective sorbents during the process of photodegradation of harmful dyes within waste water recycling practices.

KEYWORDS: Chitosan membrane, Fast Green FCF, photocatalytic degradation, nanocomposites ZnO/CuO, UV, solar light

RECEIVED: October 20, 2017. **ACCEPTED:** February 13, 2018.

TYPE: Original Research

FUNDING: The author(s) received no financial support for the research, authorship, and/or publication of this article.

DECLARATION OF CONFLICTING INTERESTS: The author(s) declared no potential conflicts of interest with respect to the research, authorship, and/or publication of this article.

CORRESPONDING AUTHOR: Eman Alzahrani, Chemistry Department, Faculty of Science, Taif University, 888-Taif, Kingdom of Saudi Arabia. Email: em-s-z@hotmail.com

Introduction

The textile industry makes a significant contribution to global economic development; however, it is also a significant source of environmental pollution. For example, dye manufacturers produce dyes that are formed of complex aromatic compounds that are chemically stable and exhibit low biodegradability in aquatic systems.[1–4] These dyes are potentially toxic, hazardous, and carcinogenic compounds; as such, there is a need to remove from the waste water produced during the production of textiles before it is discharged into the environment.[5–8]

Polysaccharides, such as cellulose and chitin, are the most abundant biomaterials on earth.[9] Chitosan (CS) is a significant chitin derivative that has attracted the attention of researchers in more recent years because it is environmentally friendly, soluble in aqueous media, non-toxic, biocompatible in nature, and renewable.[10–14] Furthermore, CS's chemical structure entails that it can naturally support the immobilisation of various species.[15–17] Researchers have successfully employed CS films to remove a variety of organic dyes from coloured waste water, and this approach has proven to be cost-effective and simple while also producing low levels of sludge. However, the use of a natural adsorbent (CS) to remove dyes is not without its drawbacks. Some of the disadvantages of the approach include long adsorption contact time, non-resistance against acid solution, and low adsorption capacity.[18] These shortcomings limit the practical applications of natural adsorbents and, as such, they need to be addressed through the development of more commercially viable approaches by which harmful dyes can be removed from waste water.[19,20]

In recent years, researchers have focused on the use of semiconductor photocatalysts to photodegrade harmful dyes because they demonstrate the ability to completely degrade such colourants.[21,22] Zinc oxide (ZnO) nanoparticles are commonly used as photocatalysts due to their unique physical and chemical properties; for example, they are non-toxic and have high chemical stability, broad absorption, high photostability, and are cost-effective in comparison with the alternative nano-sized metal oxides that are available.[7,23–25] In addition, their broad direct energy band makes them suitable for use as a semiconductor photocatalyst.[26–29] However, the absorption range of ZnO nanoparticles is limited to a narrow range of the solar spectrum; specifically, the UV region. As such, it exhibits low photocatalytic efficiency. In an attempt to overcome this, some researchers have loaded metals onto the surface of the ZnO nanoparticles to enhance the photocatalytic efficiency of the metal oxides and improve the efficiency of the use of the visible light by trapping the photoexcited electrons and subsequently

transferring them to the metal oxides.[30,31] Researchers have developed a specific interest in techniques that involve loading copper oxide (CuO) onto the surface of ZnO nanoparticles because CuO is chemically stable in atmospheric conditions and during photocatalytic reactions.[32–34]

Nanomaterials tend to agglomerate to decrease their surface area and surface energy, and this can directly influence their performance. To overcome this, a matrix can be employed to act as a support that diminishes the reduction of surface area and inhibit the aggregation of nanomaterials.[5,35] ZnO/CuO composites have been studied as potential photocatalysts for the removal of dyes.[36–41] However, to the best of our knowledge, no work has yet been performed that has specifically investigated the immobilisation of these nanocomposites on a CS membrane for use within dye removal applications. Adding nanocomposites to a CS polymer can enhance its properties. As such, this study investigated the preparation of a CS film for use as a matrix phase, whereas the nanomaterials were used as photocatalysts. Four techniques were used to characterise the prepared membrane: X-ray diffraction (XRD), scanning electron microscopy (SEM), energy-dispersive X-ray (EDAX), and atomic force microscopy (AFM) analyses. In addition, the performance of the membrane as a photocatalyst was evaluated using FCF as a model dye for tests under solar light and UV light irradiation.

Experiment

Chemicals and materials

Zinc acetate dihydrate [$Zn(CH_3COO)_2{\cdot}2H_2O$], oxalic acid dihydrate [$HO_2CCO_2H{\cdot}2H_2O$], CS from shrimp shells (molecular weight, 190 000-375 000 Da; degree of deacetylation, 75%), and analytical standard Fast Green FCF were purchased from Sigma-Aldrich (Poole, UK). Ethanol, copper(II) sulphate pentahydrate ($CuSO_4{\cdot}5H_2O$) (99.8%), and acetic acid were purchased from Sinopharm Chemical Reagent Co., Ltd (Beijing, China). All the chemicals were used as supplied without any further purification. The solutions were prepared using distilled water, and the same solutions were subsequently used for all the preparations. Petri plates were purchased from Fisher Scientific (Waltham, MA, USA).

Instrumentation

A magnetic stirrer and heater were purchased from Fisher Scientific Co. Ltd. (Shanghai, China). A furnace (WiseTherm high-temperature muffle furnace) was bought from Wisd Laboratory Instruments (Wertheim, Germany). X-ray diffraction patterns were obtained using a Bruker diffractometer D8-ADVANCE with $CuK_{\alpha 1}$ radiation (Coventry, UK). Energy-dispersive X-ray analysis was performed using a JEOL JSM 6390 LA Analytical device (Tokyo, Japan). The UV-Vis spectrophotometer was from Thermo Scientific GENESYS 10S (Toronto, Canada). High-resolution AFM was used to test the morphological features and to produce a topological map (Veeco-di Innova Model-2009-AFM-USA). The UV radiation source was a 100-W high-pressure mercury lamp with a wavelength of 290 to 450 nm and peak intensity of 365 nm (Model OCRS-I; Kaifeng Hxsei Science Instrument Factory, Kaifeng, China).

Fabrication of the ZnO nanoparticles

The sol-gel ZnO nanoparticles were fabricated using the method described in our previous work.[7] Briefly, 5.5 g of zinc acetate dihydrate was mixed with 150 mL of ethanol in an oil bath at 60°C under constant stirring (350 rpm). Then, 6.3 g of oxalic acid dihydrate was dissolved in 100 mL of ethanol. Oxalic acid in ethanol was then added drop-wise to the warm zinc acetate dihydrate in ethanol. The obtained gel was washed with plenty of distilled water before being dried in a vacuum oven at 80°C for 72 hours. Finally, the white product was calcined at 500°C in a muffle furnace for 4 hours.

Fabrication of the ZnO/CuO nanocomposites

The nanocomposites were fabricated via a wet impregnation method using a method described in a previous work[42] by mixing 0.5 g of the fabricated ZnO nanoparticles with an aqueous solution of 8 mol of $CuSO_4{\cdot}5H_2O$. The mixture was then stirred for 72 hours to allow the penetration of Cu^{2+} ions into the zinc oxide crystal matrix. The product was calcined at 550°C in a muffle furnace for 5 hours.

Fabrication of the thin film membrane

About 1.0 g of CS was dissolved in an aqueous acetic acid solution (2%, v/v). The mixture was then stirred at 700 rpm at 30°C for 24 hours to obtain a homogeneous solution before being filtered through a nylon cloth to remove any undissolved material. Then, 0.05 g of ZnO nanoparticles or ZnO/CuO nanocomposites was added to 20 mL of the previous solution, which was then stirred at 700 rpm at 30°C for 24 hours. Finally, 10 mL of the formed solution was cast onto a Petri plate and dried at room temperature. Once completely dry, the membranes were ready to use.

Characterisation of the prepared materials

Phase identification and structural analysis were performed using XRD with Cu Ka radiation (=1.5405 Å) in the 2-theta (2θ) range from 5° to 80°. The surface morphology of the fabricated ZnO nanoparticles was characterised by SEM analysis after coating the samples with a thin layer of gold to prevent charge problems and enhance the resolution. Compositional analysis was performed using EDAX analysis. The fabricated materials were imaged by an AFM instrument to determine the sample thickness.

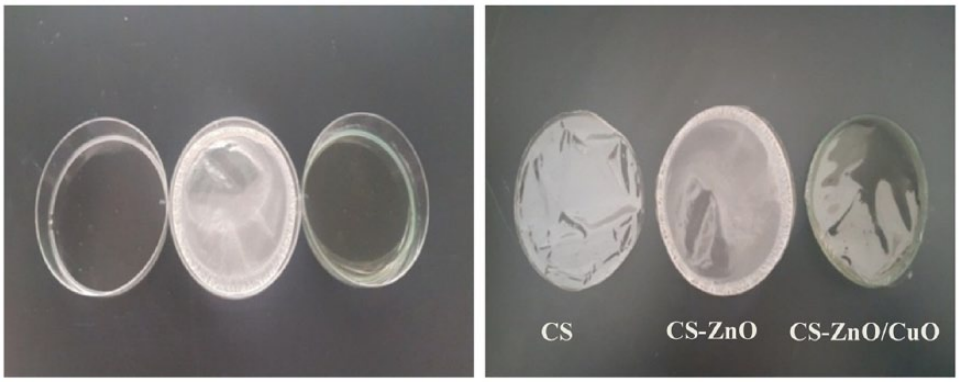

Figure 1. Images of the fabricated thin film membranes before (left) and after (right) peeling from the Petri dishes. CS indicates chitosan; CuO, copper oxide; ZnO, zinc oxide.

Degradation of FCF

The photocatalytic experiments were conducted at ambient temperature by placing the film in a beaker (Pyrex) that contained 100 mL of FCF dye (30 mg L^{-1}). The solution was magnetically stirred at 500 rpm in the dark to reach the adsorption-desorption equilibrium. After 1 hour, the degradation experiment was performed under sunlight or with the UV lamp (365 nm) at different light exposure times (0-110 minutes). Solar light reactions were performed on a house roof in Taif City between 11 AM and 1 PM, and the intensity of the solar light irradiation was 1150 W m^{-2}.[43,44] Aliquots of 2 mL were extracted with the aid of a syringe at 5-minute intervals for immediate analysis.

The concentration of FCF was determined using a UV-Vis spectrophotometer in the range of between 350 and 800 nm. The decolourisation efficiency (%) was calculated using equation (1)[45–48]:

$$\text{Degradation percentage}(\%) = 100 \times \frac{(C_o - C)}{C_o} = 100 \times \frac{(A_o - A)}{A_o} \quad (1)$$

where C_o is the initial concentration of the dye solution, C is the concentration of the dye solution after photoirradiation over a selected time interval (5 minutes), and A_o and A are the absorbance of the dye solution at the initial time and at any time period thereafter, respectively.

Results and Discussion

Characterisation of the fabricated membranes

The aim of this study was to fabricate ZnO nanoparticles and ZnO/CuO nanocomposites immobilised on a CS matrix for use during the process of photodegrading FCF dye. The thin film membrane was prepared in an acetic acid medium using the solvent casting method.[49] Figure 1 shows the appearance of the fabricated films before and after peeling from the Petri dishes. As can be seen, the prepared CS membranes were thin, flexible, smooth, and transparent. The same result was obtained by Azad et al[50] and Averineni et al.[51] The colour of the CS membrane that contained ZnO nanoparticles was white, whereas the colour of the CS membrane that contained ZnO/CuO nanocomposites was green.

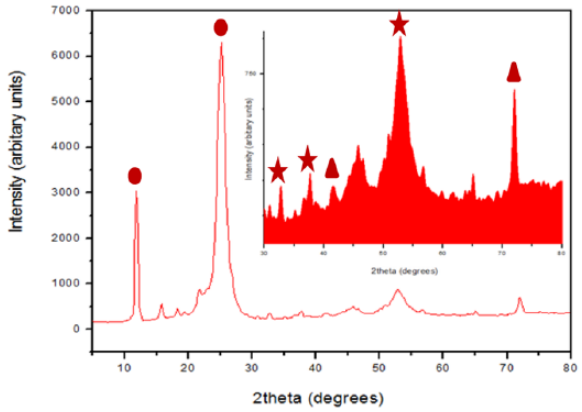

Figure 2. X-ray diffraction pattern of the CS-ZnO/CuO membrane (circle) chitosan, (star) CuO, and ZnO (triangle). CS indicates chitosan; CuO, copper oxide; ZnO, zinc oxide.

The X-ray powder diffraction (XRD) pattern of the CS-ZnO/CuO membrane is shown in Figure 2. The two strong peaks in the diffractogram of 2θ at 11.80° and 25.29° were ascribed to CS, highlighting the high degree of crystallinity of the membrane, whereas the XRD of the CS membrane was characteristic of an amorphous polymer.[52–55] The diffraction peaks of 2θ at 33.34°, 37.96°, and 53.32° were ascribed to tenorite and monoclinic CuO.[35,56] In addition, diffraction peaks belonging to the hexagonal structure of ZnO were observed for 2θ at 46.36° and 72.52°.[7,57,58] However, not all the diffraction peaks of ZnO and CuO were fully resolved due to the lower concentration of CuO on the membrane and/or the overlap between these peaks and those of CS.

The fabricated film membranes were studied using SEM analysis, and the electron microscopy images are presented in Figure 3. As Figure 3A indicates, the structure of the CS membrane was homogeneous and exhibited smooth surfaces and

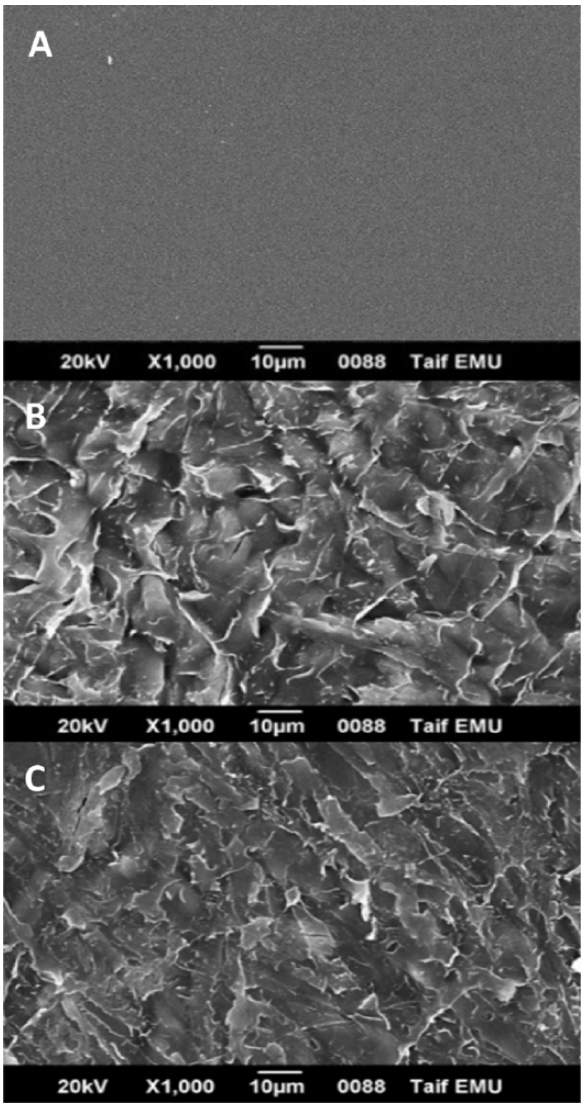

Figure 3. Morphology of (A) CS film, (B) CS-ZnO membrane, and (C) CS-ZnO/CuO membrane by scanning electron microscopic observation. CS indicates chitosan; CuO, copper oxide; ZnO, zinc oxide.

without pores or cracks. Similar results have been previously reported.[59] However, the electron microscopy images of the CS-ZnO membrane (Figure 3B) and the CS-ZnO/CuO membrane (Figure 3C) revealed that the immobilisation of the nanomaterials in the CS membranes led to an increase in the surface roughness and the formation of numerous holes. In addition, it was found that the roughness of CS membrane containing ZnO/CuO nanocomposite was more than that of CS membrane containing ZnO nanoparticles. The roughness and presence of holes indicated that the biopolymer network had undergone a change that led to the development of high porosity and a large active surface area.[60]

The EDAX analysis was performed on the synthesised membranes to identify the chemical composition of the fabricated materials. Figure 4 shows the EDAX spectra of the CS membrane, the CS membrane containing ZnO nanoparticles, and the CS membrane containing ZnO/CuO nanocomposites between 0 and 10 kV. As can be observed in Figure 4A, the EDAX spectrum of the CS membrane showed strong peaks of carbon (C) at 0.277 keV and oxygen (O) at 0.525 keV.[12] Three peaks related to zinc in the tested material were observed in the CS membrane containing ZnO nanoparticles for the zinc (Zn) element, Zn L_α, Zn K_α, and Zn K_β (Figure 4B), and this confirms the existence of ZnO nanoparticles.[7,61,62] The EDAX spectrum of the ZnO/CuO nanocomposites embedded in the CS membrane (Figure 4C) revealed that, in addition to the peaks for the C, O, and Zn elements, a new peak was observed at 8.040 keV that was related to copper (Cu). These results confirmed that a CuO layer had been successfully loaded on the ZnO nanoparticles. The source of Au (at 2.12 keV) in the EDAX spectra corresponds to the Au coating used for the characterisation.

Table 1 presents the composition of 59.35% carbon and 40.65% oxygen in the CS membrane sample, while 8.39% zinc was found in the CS film containing ZnO nanoparticles, and 1.28% copper was found in the CS membrane containing ZnO/CuO nanocomposites, without any elemental impurities present in the fabricated materials. The low concentration of CuO in the latter membranes exhibited a good agreement with the result obtained from the XRD analysis.

To access qualitative and quantitative information pertaining to the diameter of the synthesised membranes, the surface properties of the synthesised membranes were studied using AFM.[63–66] Figure 5 shows the 3-dimensional (3D) AFM images of the fabricated materials obtained using AFM. As can be clearly observed, the flat surface of the CS membrane was smooth and uniform, with an average particle size of 23.1 nm. However, after embedding the ZnO nanoparticles, the surface roughness increased to 36.6 nm. The 3D AFM image of the ZnO/CuO nanocomposites–embedded CS membrane showed that the roughness increased to 41.2 nm, confirming the presence of the nanocomposites in the CS membrane.

Evaluation of the photocatalytic performance

Degradation under solar light. The photocatalytic activities of the fabricated membranes were evaluated by decolourising a heterocyclic dye, namely, Fast Green FCF, under solar light. To verify the photocatalytic activities of the fabricated membranes, each membrane was placed in a beaker containing 100 mL of the FCF solution (30 mg L^{-1}). Before being exposed to the solar light, the mixture was magnetically stirred at 500 rpm. The experiment was performed in the dark to establish an adsorption-desorption equilibrium between the dye and the surface of the photocatalyst under normal atmospheric conditions.[67–70] The suspension was then magnetically stirred and exposed to solar light for different irradiation times ranging between 0 and 11 minutes. At every 5-minute interval, an aliquot of 2 mL was withdrawn from the beaker to determine the dye concentration.

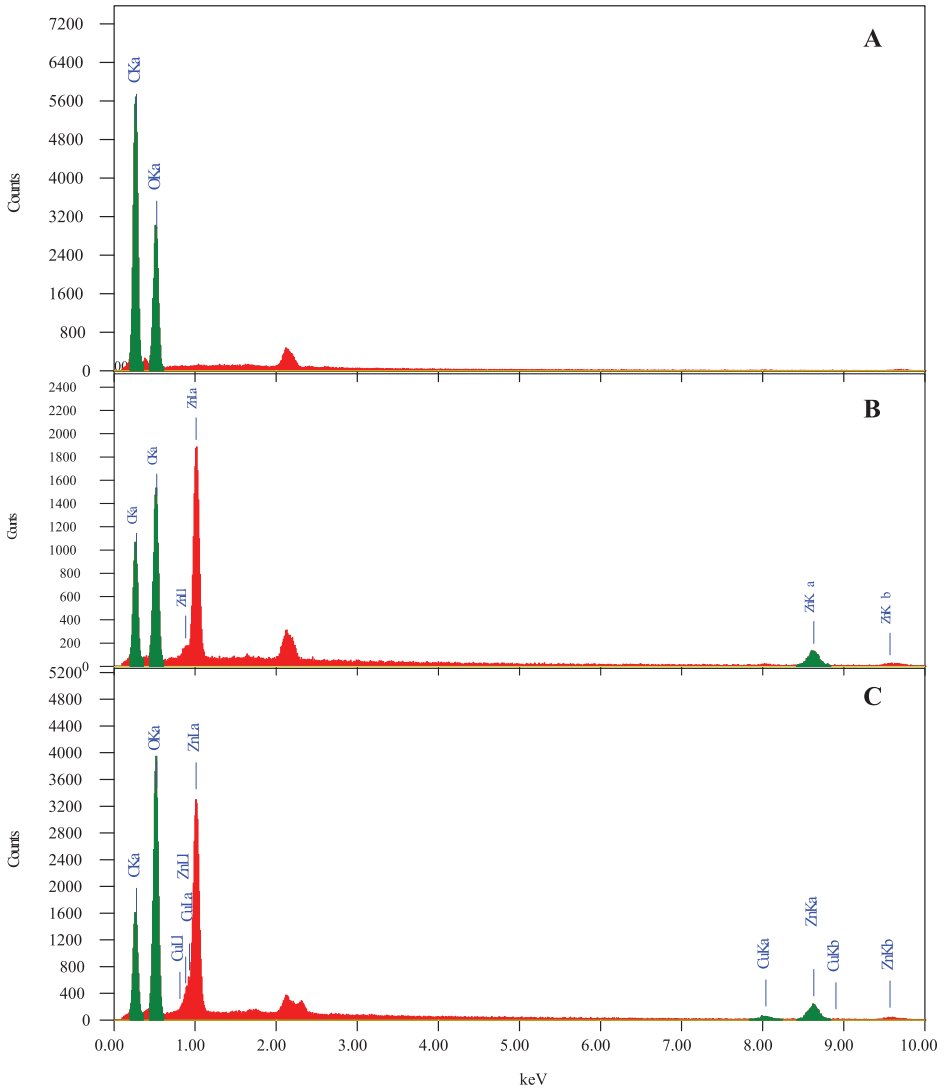

Figure 4. Energy-dispersive X-ray spectra of (A) CS membrane, (B) CS membrane containing ZnO nanoparticles, and (C) CS membrane containing ZnO/CuO nanocomposites. CS indicates chitosan; CuO, copper oxide; ZnO, zinc oxide.

Table 1. Elemental composition of the fabricated materials determined by energy-dispersive X-ray analysis.

SAMPLE	ELEMENT				TOTAL
	C	O	Zn	Cu	
CS membrane	59.35	40.65	0	0	100.00
CS-ZnO membrane	51.76	39.85	8.39	0	100.00
CS-ZnO/CuO membrane	43.76	46.64	8.32	1.28	100.00

Abbreviations: CS, chitosan; CuO, copper oxide; ZnO, zinc oxide.

Figure 6 presents the photographic images that represent the change in the colour of the FCF dye during the photodegradation experiments in which fabricated membranes were employed over different irradiation times under solar light. The dye solution should be bright sea green. No degradation of FCF was observed when the CS membrane was used as the photocatalyst. In fact, the bright sea green colour of the dye actually increased. However, when the CS-ZnO and CS-ZnO/CuO membranes were employed as the photocatalysts, the colour of the FCF dye steadily decreased in response to the increase in exposure time to solar light, indicating the decomposition of the dye.

Qualitative information related to the intermediates formed during the photodegradation was obtained from the absorbance spectrum in the region between 350 and 800 nm, whereas the quantitative information was obtained by calculating the

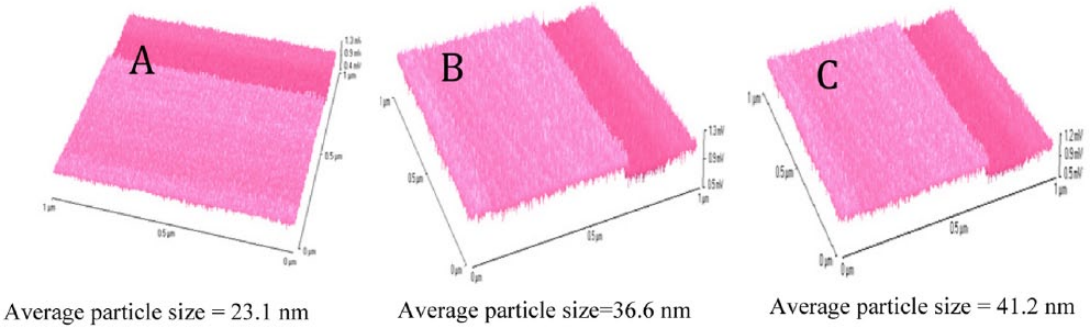

Figure 5. Atomic force microscopy of (A) CS membrane, (B) ZnO nanoparticles embedded CS membrane, and (C) ZnO/CuO nanocomposites–embedded CS membrane. CS indicates chitosan; CuO, copper oxide; ZnO, zinc oxide.

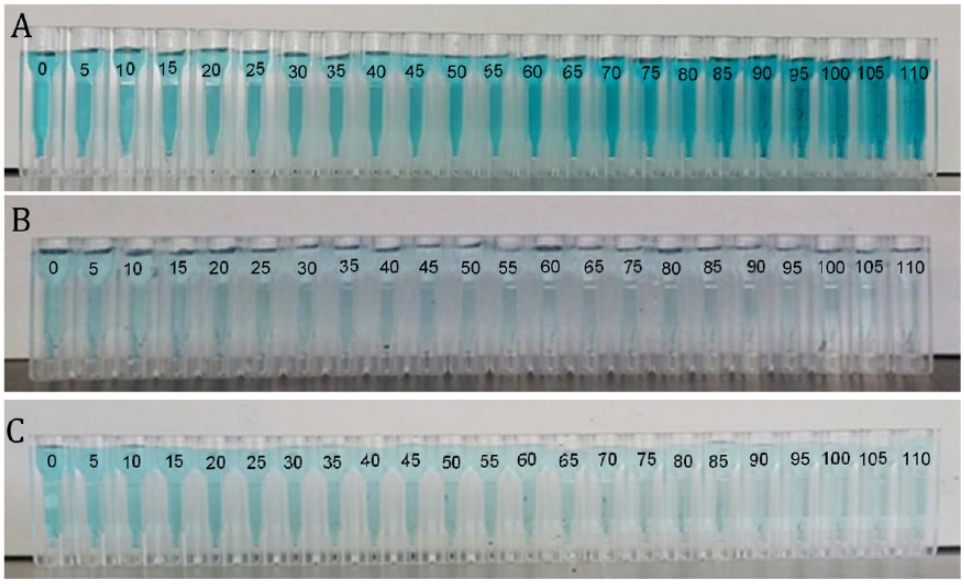

Figure 6. Photographic image representing the change in colour of FCF during photodegradation for different irradiation times (0-110 minutes) under solar light using (A) CS membrane, (B) CS-ZnO membrane, and (C) CS-ZnO/CuO membrane. CS indicates chitosan; CuO, copper oxide; ZnO, zinc oxide.

decrease in the absorption intensity of FCF at a λ_{max} of around 623 nm.[71,72] The changes in the FCF absorption spectra as a function of irradiation time were recorded using a UV-Vis spectrometer and are presented in Figure 7, which presents the UV-Vis spectra of FCF at 5-minute intervals over a 110-minute period recorded using a UV-Vis spectrophotometer in the presence of CS membrane (Figure 7A), CS membrane containing CS-ZnO (Figure 7B), and CS-ZnO/CuO membrane as photocatalysts (Figure 7C). As can be seen in Figure 7A, the characteristic absorption peaks of FCF decreased until 35 minutes of exposure to solar light. The characteristic absorption peaks of FCF then increased until 110 minutes reaction time. These results could be attributed to the rupture of the CS membrane during the experiment, which could have affected the photocatalytic activity of the film membrane. In the case of the CS membrane embedded with ZnO nanoparticles (Figure 7B) and the membrane embedded with ZnO/CuO nanocomposites (Figure 7C), the characteristic absorption peaks of the Fast Green FCF decreased gradually in response to an increase in the irradiation time and exposure to solar light from 0 to 110 minutes, without exhibiting additional absorption features and with no breakage of the prepared film membranes. The gradual reduction in the absorbance of the FCF dye over time indicated that the prepared membranes contributed to the gradual photodegradation of FCF.[73]

Table 2 shows the wavelength and the absorbance of the FCF dye at 5-minute intervals together with details of the degradation percentage of the dye. A hypsochromic shift (ie, a blue shift of the band gap) in the absorption wavelength was observed when the CS membrane was used, whereas the positions of the absorbance peaks of the FCF dye were shifted bathocromically (ie, a red shift of the band gap) when the CS-ZnO and CS-ZnO/CuO membranes were used. In addition, the CS membrane embedded with ZnO nanoparticles achieved a 57.90% degradation efficiency, whereas the CS-ZnO/CuO membrane reached an efficiency of 60.23% within 110 minutes of the reaction. The results, therefore, indicated that the CS membranes embedded with ZnO/CuO nanocomposites achieved an enhanced photocatalytic activity in terms of efficiency under solar light irradiation than the

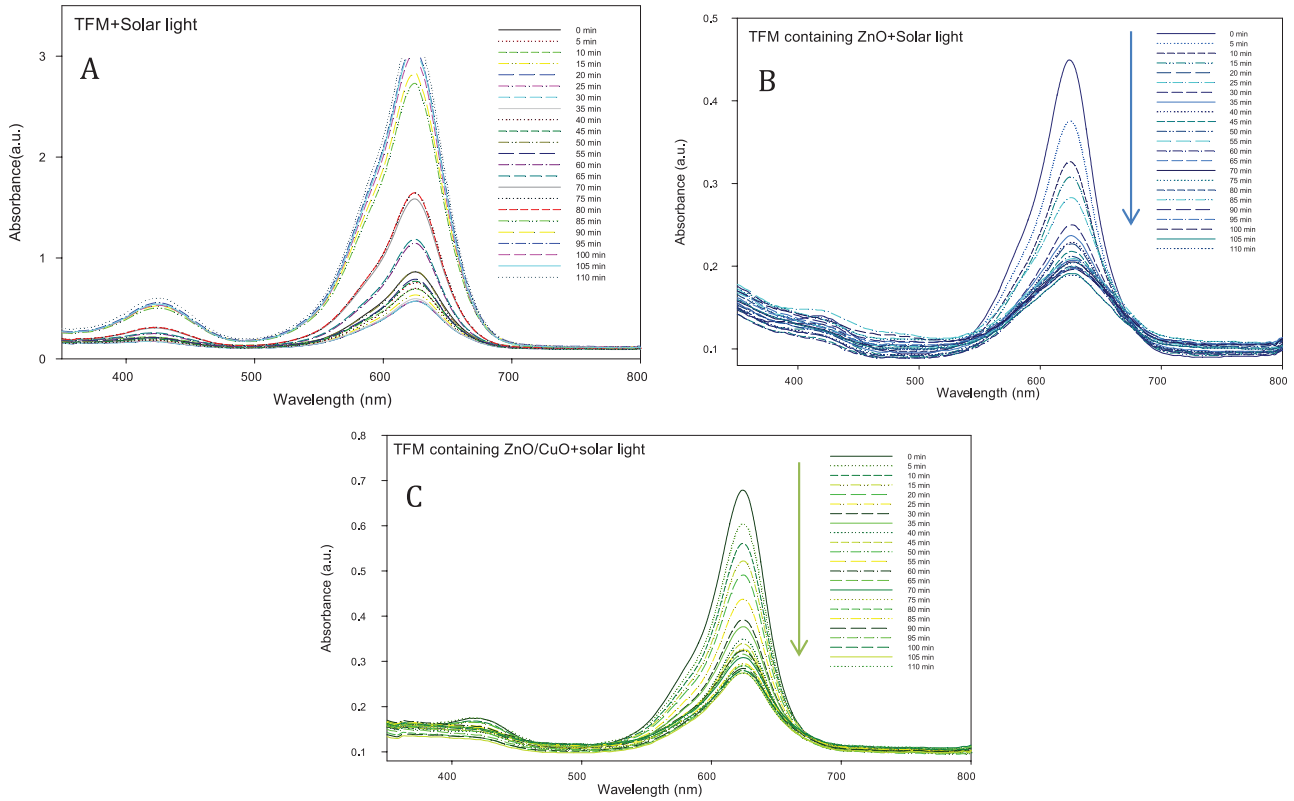

Figure 7. Absorption spectra of FCF (30 mg L^{-1}) at different times (0-110 nm) after exposure to solar light using (A) CS membrane, (B) CS membrane containing ZnO nanoparticles, and (C) CS membrane containing ZnO/CuO nanocomposites as photocatalysts.

Table 2. Photochemical degradation of FCF under solar light using the fabricated membranes: W (wavelength), A (absorbance), and D (degradation).

TIME, MIN	CS MEMBRANE			CS-ZnO MEMBRANE			CS-ZnO/CuO MEMBRANE		
	W, NM	A, A.U.	D, %	W, NM	A, A.U.	D, %	W, NM	A, A.U.	D, %
0	626	0.860	00.00	623	0.449	00.00	623	0.684	00.00
5	626	0.754	12.32	626	0.375	16.48	623	0.604	11.69
10	626	0.692	19.53	626	0.326	27.39	623	0.560	18.12
15	626	0.632	26.51	626	0.308	31.40	623	0.521	23.83
20	626	0.589	31.51	626	0.294	34.52	623	0.490	28.36
25	626	0.573	33.37	626	0.283	36.97	623	0.437	36.11
30	626	0.571	33.60	626	0.261	41.87	623	0.392	42.69
35	626	0.595	30.81	626	0.250	44.32	623	0.376	45.02
40	626	0.698	18.83	626	0.237	47.21	623	0.349	48.97
45	626	0.768	10.69	626	0.227	49.44	623	0.339	50.43
50	626	0.788	8.370	626	0.212	52.78	626	0.327	52.19
55	626	0.866	−0.69	626	0.209	53.45	626	0.325	52.48
60	626	1.143	−32.90	629	0.207	53.89	626	0.323	52.77
65	626	1.182	−37.44	629	0.206	54.12	626	0.316	53.80
70	623	1.582	−83.95	629	0.205	54.34	626	0.308	54.97
75	623	1.641	−90.81	629	0.204	54.56	626	0.292	57.30

(Continued)

Table 2. (Continued)

TIME, MIN	CS MEMBRANE			CS-ZnO MEMBRANE			CS-ZnO/CuO MEMBRANE		
	W, NM	A, A.U.	D, %	W, NM	A, A.U.	D, %	W, NM	A, A.U.	D, %
80	623	1.642	−90.93	629	0.200	55.45	626	0.290	57.60
85	623	2.724	−216.74	629	0.199	55.67	626	0.285	58.33
90	623	2.830	−229.07	629	0.198	55.90	626	0.284	58.47
95	Out of range			629	0.197	56.12	626	0.280	59.06
100	Out of range			629	0.196	56.34	626	0.279	59.21
105	Out of range			629	0.191	57.46	626	0.274	59.94
110	Out of range			629	0.189	57.90	626	0.272	60.23

Abbreviations: CS, chitosan; CuO, copper oxide; ZnO, zinc oxide.

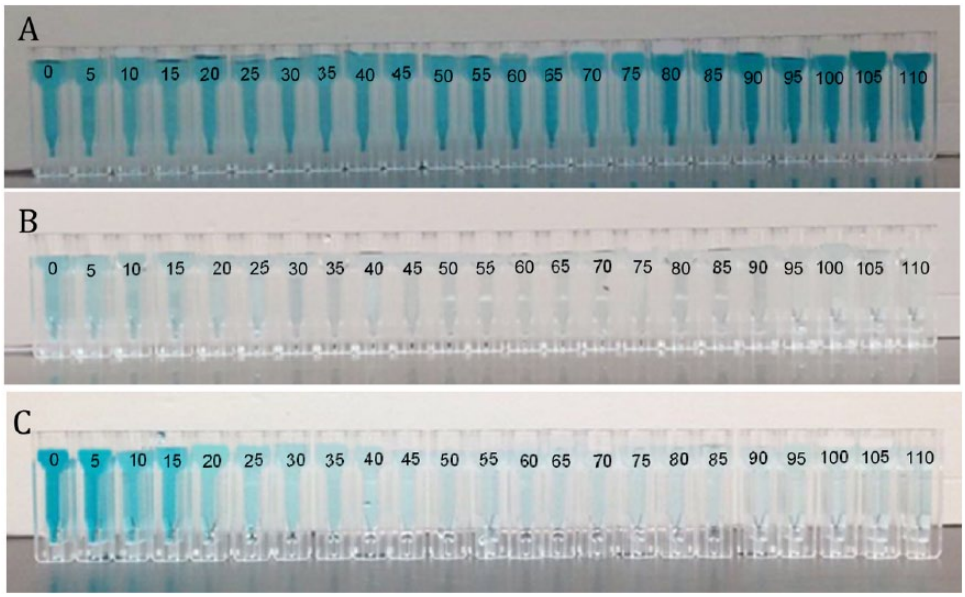

Figure 8. Photographic image representing the change in colour of FCF during photodegradation for different irradiation times (0-110 minutes) under UV light irradiation (365 nm) using (A) CS membrane, (B) CS-ZnO membrane, and (C) CS-ZnO/CuO membrane. CS indicates chitosan; CuO, copper oxide; ZnO, zinc oxide.

other prepared membranes. The photodegradation efficiency of FCF did not increase as the reaction time increased. This could be attributed to the accumulation of the dye on the surface of the catalyst and is in agreement with previous research that has found that the photocatalytic degradation of different dyes ceases after a certain period of degradation.[34,74]

Degradation under UV light. The photocatalytic activities of the fabricated membranes were also examined under UV light irradiation (365 nm) using the same procedure as that used for the degradation of FCF under solar light. Figure 8 presents a photograph that exhibits the change in the colour of the FCF solution in response to increased photodegradation time. As the figure indicates, the colour of the FCF dye did not change when the CS membrane was used as a photocatalyst under UV light irradiation, indicating a poor photocatalytic activity for the photodegradation of the FCF dye. However, the colour of the dye changed from a bright sea green to become nearly transparent at the end of the degradation process when the CS-ZnO or CS-ZnO/CuO membranes were employed, indicating the destruction of the chromophoric structure and the complete photodegradation of the dye.

The degradation processes were evaluated in accordance with the change in absorbance at the maximum absorption wavelength by monitoring the maximum wavelengths (λ_{max}) of FCF at 623 nm for different irradiation times (0-110 minutes) using a UV-Vis spectrophotometer in the range of 350 to 800 nm. Figure 9 shows the UV-Vis spectra of the FCF in aqueous solution as a function of irradiation time under UV light irradiation. As can be observed in Figure 9A, the UV-Vis absorption peaks corresponding to the FCF dye gradually decreased as the exposure time to UV light irradiation increased.

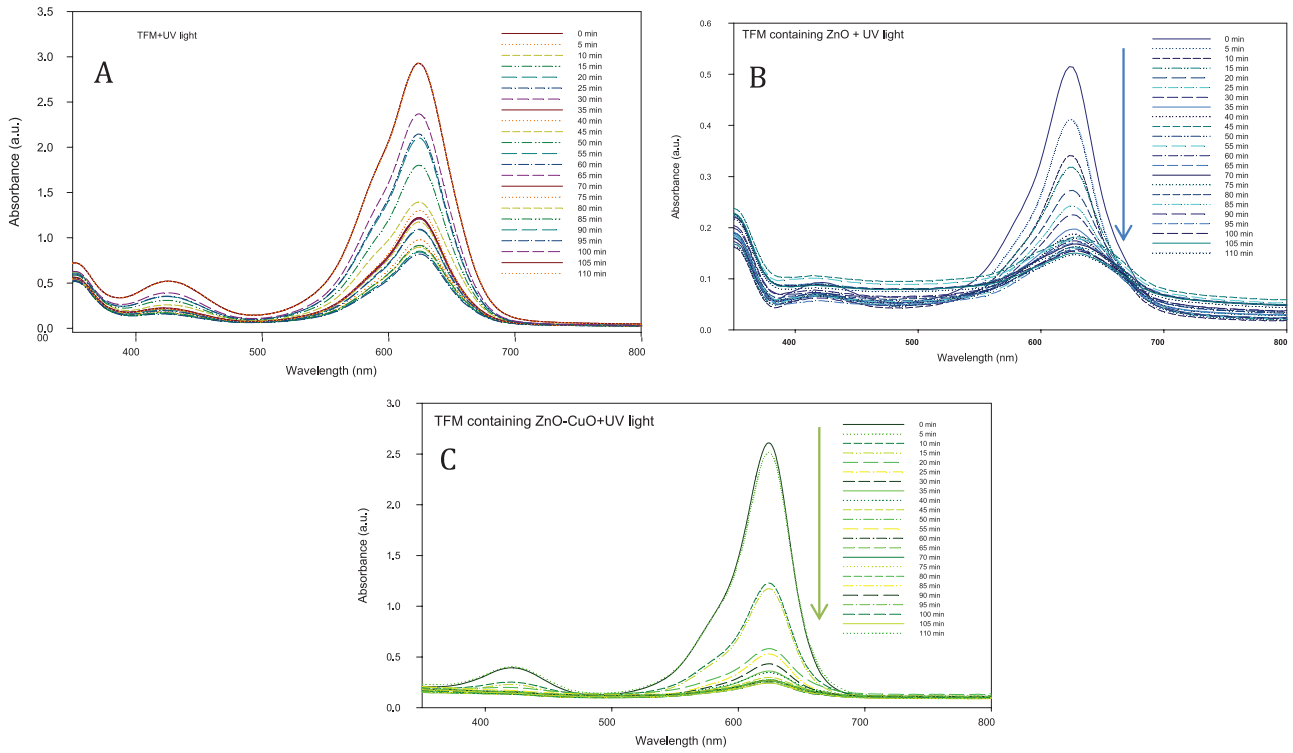

Figure 9. Absorption spectra of FCF (30 mg L^{-1}) at different times (0-110 nm) after exposure to UV light irradiation (365 nm) using (A) CS membrane, (B) CS membrane containing ZnO nanoparticles, and (C) CS membrane containing ZnO/CuO nanocomposites as photocatalysts. CS indicates chitosan; CuO, copper oxide; ZnO, zinc oxide.

However, after 30 minutes of irradiation, the absorption peaks of the FCF dye increased. In contrast, when the CS-ZnO (Figure 9B) or CS-ZnO/CuO (Figure 9C) membranes were used in the absorption process, a reduction in the absorbance bands in response to the increase in the UV light irradiation time from 0 to 110 minutes was observed. Furthermore, the absorbance peaks of the FCF dye almost disappeared at 110 minutes exposure to UV light irradiation but no other absorption features were detected by the UV-Vis spectrophotometer, thereby confirming the degradation of the FCF dye.

Table 3 presents the change in the peak position and absorbance of the FCF dye together with the photodegradation percentage of FCF for the fabricated membranes at different irradiation times. The photodegradation efficiency of the CS membrane increased until 30 minutes of reaction, reaching 26.44%, before the photodegradation efficiency started to decrease. The lower performance of the CS membrane could be attributed to the instability of the CS membrane, which ruptured during the experiment. However, the CS-ZnO and CS-ZnO/CuO membranes did not change. In addition, the degradation percentage of the dye increased in response to the increase in the irradiation time when the CS-ZnO and CS-ZnO/CuO membranes were used. The degradation percentage of the Fast Green FCF dye was 71.45% when the CS-ZnO membrane was used, whereas the use of the CS-ZnO/CuO membrane resulted in an even greater increase in the photodegradation efficiency and degradation capability, decomposing 91.21% of FCF in 110 minutes. Furthermore, the efficiency was maintained at this value as the reaction continued. The results also demonstrated that there was a shift in the position of the peak-to-longer wavelength (ie, a red shift of the band gap) when the CS-ZnO or CS-ZnO/CuO membranes were used, whereas the position of the peak fluctuated when the CS membrane was used.

Photodegradation rate. The degradation kinetics of the FCF dye were calculated and are depicted in Figure 10, which presents the plot of C/C_o versus irradiation time, where C is the absorption of FCF at a wavelength of 623 nm at a particular time interval and C_o is the absorption after the adsorption equilibrium of the sample before irradiation ($t=0$). The degradation kinetics of FCF indicate that the CS membrane containing ZnO/CuO nanocomposites achieved the most effective performance in terms of the removal of FCF from an aqueous solution in the presence of solar light irradiation and UV light irradiation, reaching 60.23% and 91.21% decolourisation efficiency, respectively, over a 110-minute duration in comparison with the CS/ZnO membrane which achieved 57.90% and 71.45% decolourisation in the presence of solar light and UV light irradiation, respectively.

The photocatalytic degrading capability of the CS-ZnO/CuO membrane compared with the CS-ZnO membrane could be attributed to the doping of a CuO narrow band gap semiconductor on the surface of the ZnO semiconductor nanoparticles. Furthermore, using different semiconductors could enhance the charge separation and increase the lifetime of the charge carriers. The work function of Cu (4.9 eV) is smaller

Table 3. Photochemical degradation of FCF under UV light irradiation using the fabricated membranes: W (wavelength), A (absorbance), and D (degradation).

TIME, MIN	CS MEMBRANE			CS-ZnO MEMBRANE			CS-ZnO/CuO MEMBRANE		
	W, NM	A, A.U.	D, %	W, NM	A, A.U.	D, %	W, NM	A, A.U.	D, %
0	623	1.093	00.00	623	0.515	00.00	623	2.607	00.00
5	626	0.914	16.37	623	0.412	20.00	623	2.516	3.49
10	626	0.896	18.02	623	0.341	33.78	623	1.227	52.93
15	626	0.851	22.14	626	0.318	38.25	623	1.171	55.08
20	626	0.841	23.05	626	0.273	46.99	626	0.581	77.71
25	626	0.819	25.06	626	0.243	52.81	626	0.529	79.70
30	626	0.804	26.44	626	0.225	56.31	626	0.432	83.42
35	626	0.925	15.37	629	0.197	61.74	626	0.361	86.15
40	632	0.977	10.61	629	0.188	63.49	626	0.347	86.68
45	623	0.996	8.87	629	0.180	65.04	626	0.298	88.56
50	626	1.017	6.95	629	0.178	65.43	626	0.277	89.37
55	626	1.085	0.73	629	0.174	66.21	626	0.272	89.56
60	626	1.173	–7.31	629	0.170	66.99	626	0.271	89.60
65	623	1.208	–10.52	629	0.168	67.37	626	0.270	89.64
70	623	1.221	–11.71	629	0.165	67.96	626	0.269	89.68
75	626	1.300	–18.93	629	0.163	68.34	626	0.268	89.71
80	623	1.393	–27.44	629	0.162	68.54	626	0.267	89.75
85	623	1.800	–64.68	629	0.160	68.93	626	0.266	89.79
90	623	2.101	–92.22	629	0.158	69.32	626	0.263	89.91
95	623	2.145	–96.24	629	0.156	69.70	626	0.262	89.95
100	623	2.367	–116.56	629	0.154	70.09	626	0.246	90.56
105	623	2.924	–167.52	629	0.150	70.87	626	0.242	90.71
110	623	2.926	–167.70	629	0.147	71.45	626	0.229	91.21

than that of ZnO (5.3 eV)[34,75] and this promotes the transfer of the photoexcited electrons from CuO (more cathodic valence band than the valence band of ZnO) to the ZnO conduction band (more anodic valence band) with a reduction in the oxygen vacancies of the nanocomposites. This is supported by the electron affinities of Cu (1.235 eV) and ZnO (2.087 eV), whereas the hole transfer from ZnO to the valence band of CuO is in competition with electron-hole recombination in the respective semiconductors[34,42,66,76]:

$$CuO\left(e^- + h^+\right) + ZnO\left(e^- + h^+\right) \rightarrow$$
$$CuO\left(h^+ + h^+\right) + ZnO\left(e^- + e^-\right)$$
$$ZnO\left(e^-\right) + FCF \rightarrow photobleached\ \ products$$
$$CuO\left(h^+\right) + FCF \rightarrow photobleached\ \ products$$

Therefore, the doping of CuO on the surface of ZnO semiconductor nanoparticles can improve the photocatalytic degradation of Fast Green FCF.

Reproducibility of the membranes. It was very important to check the lifetime and reusability of the fabricated membranes as a means of better understanding the cost of the treatment. The calcination method is commonly used for the regeneration of the photocatalyst[77–79]; however, this method could not be used in this study because the matrix was an organic material that could affect the film. Filice et al[80] boiled a Nafion membrane that had previously been used to remove methyl orange dye in a regeneration experiment in distilled water for 15 minutes and then dried it at 80°C for 30 minutes. The same procedure was used in this study. After the membranes had been used, they were taken from the reaction beaker and soaked in distilled water for 1 hour, air

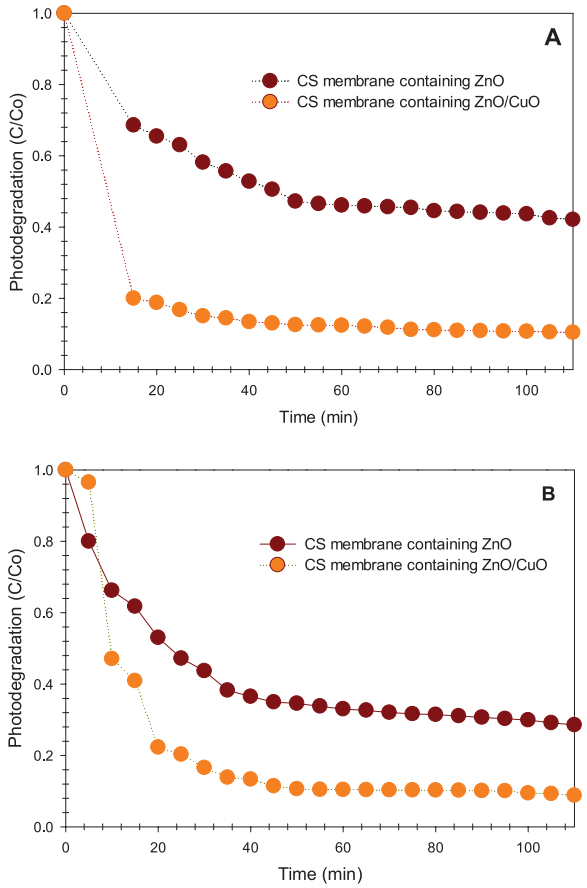

Figure 10. Degradation kinetics of FCF with respect to time (C_o and C are the equilibrium concentrations of the dye before and after photodegradation, respectively). The top curve represents FastGreen FCF mixed with the CS-ZnO membrane and CS-ZnO/CuO membrane, respectively, exposed to solar light. The bottom curve corresponds to Fast Green FCF mixed with the CS-ZnO membrane and CS-ZnO/CuO membrane, respectively, exposed to UV light irradiation. CS indicates chitosan; CuO, copper oxide; ZnO, zinc oxide.

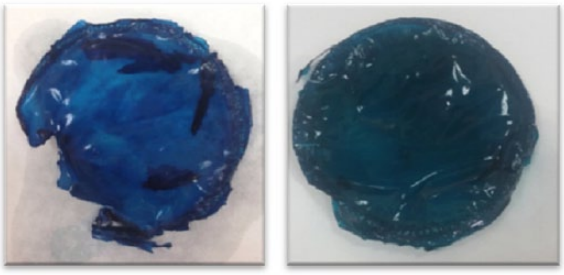

Figure 11. Photos of films taken after using the membrane for 3 cycle runs: CS-ZnO membrane (left) and CS-ZnO/CuO membrane (right). CS indicates chitosan; CuO, copper oxide; ZnO, zinc oxide.

dried, and then reused to investigate their reusability. Figure 11 presents the photographs of the membranes over three recycling photocatalysis runs. The images indicate that the appearance of the CS-ZnO/CuO membrane remained constant, whereas the CS-ZnO membrane deteriorated.

It is well known that separating the nanomaterials that have been used for degradation of target analytes after use is not an

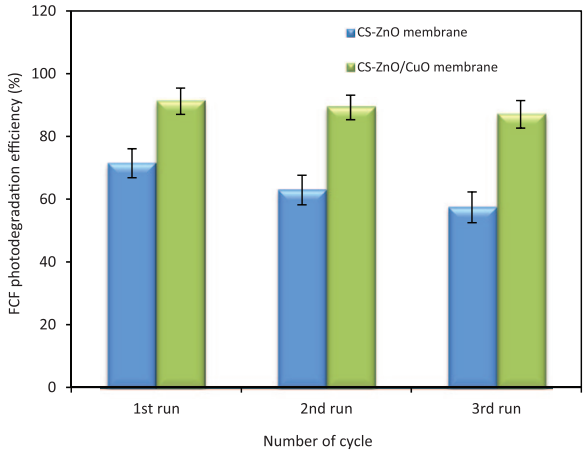

Figure 12. Reproducibility tests of the CS-ZnO membrane and CS-ZnO/CuO membrane catalyst. Decomposition percentage of Fast Green FCF versus time as a function of the cycle number. CS indicates chitosan; CuO, copper oxide; ZnO, zinc oxide.

easy task, can result in the pollution of the treated water (the photocatalytic system), and can increase the cost of their practical application. In this study, separating the catalyst from the film membrane after use was simple. In addition, centrifuge or filtration was not required to separate the nanomaterials from the treated water system.

Figure 12 presents the stability evaluation of the membranes in FCF photodegradation for three recycling photocatalysis runs under UV light irradiation. During the regeneration cycle, the photodegradation percentage of FCF using the CS-ZnO membrane decreased to 62.92% and 57.40% for the second and third cycles, respectively, whereas the photodegradation percentage of FCF using the CS-ZnO/CuO membrane decreased to 89.22% and 87.04% for the second and third cycles, respectively. The decline in the degradation rate achieved by the fabricated membrane could be attributed to the fact that the surface of the membrane became covered with dye, which can be difficult to remove and results in a reduction in the photodegradation efficiency.[81,82] However, the relatively good repeatability of the fabricated membranes (RSD < 5) can make them a potential recyclable candidate as a photocatalyst for the removal of organic pollutants from waste water. In addition, they exhibit excellent stability under UV light irradiation.

Conclusions

The membranes of CS, CS-ZnO, and CS-ZnO/CuO were successfully fabricated. The photodegradation of FCF solution was studied using the fabricated membranes. The results indicated that the photocatalytic activities of the fabricated membranes were greater in the presence of UV light irradiation than they were under solar light. In addition, the photocatalytic results indicated that the fabricated CS-ZnO/CuO membrane achieved a better UV light irradiation response than the CS and CS-ZnO membranes. The feasibility of recycling the prepared membranes was examined and the results indicated that

the CS-ZnO/CuO membrane continued to achieve a rate of photodegradation of FCF of around 87.04% even after the film had been used 3 times. Moreover, the experimental results of this study clearly demonstrated the successful photodegradation of FCF using the CS-ZnO/CuO membrane under solar light (60.23%). Further investigations to improve the photodegradation of FCF using the fabricated membranes under solar light should be performed because solar light is safe, cheap, and available throughout the year.

REFERENCES

1. Verma AK, Dash RR, Bhunia P. A review on chemical coagulation/flocculation technologies for removal of colour from textile wastewaters. *J Environ Manage*. 2012;93:154–168.
2. Sarayu K, Sandhya S. Current technologies for biological treatment of textile wastewater – a review. *Appl Biochem Biotech*. 2012;167:645–661.
3. Chequer FMD, de Oliveira DP, Ferraz ERA, de Oliveira GAR, Cardoso JC, Zanoni MVB. Textile dyes: dyeing process and environmental impact [published online ahead of print January 16, 2013]. *INTECH Open Access*. doi:10.5772/53659.
4. Kanagaraj J, Senthilvelan T, Panda R, Kavitha S. Eco-friendly waste management strategies for greener environment towards sustainable development in leather industry: a comprehensive review. *J Clean Prod*. 2015;89:1–17.
5. Motlagh MM, Hassanzadeh-Tabrizi SA, Saffar-Teluri A. Sol–gel synthesis of Mn2O3/Al2O3/SiO2 hybrid nanocomposite and application for removal of organic dye. *J Sol-Gel Sci Tech*. 2015;73:9–13.
6. Elwakeel KZ, Guibal E. Arsenic(V) sorption using chitosan/Cu(OH)2 and chitosan/CuO composite sorbents. *Carbohydr Polym*. 2015;134:190–204.
7. Alzahrani E. Zinc oxide nanopowders prepared by the sol-gel process for the efficient photodegradation of methyl orange. *Curr Anal Chem*. 2016;12:465–475.
8. Nimkar U. Sustainable chemistry: a solution to the textile industry in a developing world. *Curr Opin Green Sust Chem*. 2018;9:13–17.
9. Avérous L, Pollet E. Novel multiphase systems based on thermoplastic chitosan: analysis of the structure-properties relationships. *AIP Conf Proc*. 2016;1713:140009.
10. Rinaudo M. Chitin and chitosan: properties and applications. *Prog Polym Sci*. 2006;31:603–632.
11. Karim Z, Mathew AP, Grahn M, Mouzon J, Oksman K. Nanoporous membranes with cellulose nanocrystals as functional entity in chitosan: removal of dyes from water. *Carbohydr Polym*. 2014;112:668–676.
12. Alzahrani E. Fabrication and characterisation of chitosan-magnetic nanoparticles and its application for protein extraction. *Int J Adv Sci Tech Res*. 2014;4:755–766.
13. Ge J, Yue P, Chi J, Liang J, Gao X. Formation and stability of anthocyanins-loaded nanocomplexes prepared with chitosan hydrochloride and carboxymethyl chitosan. *Food Hydrocol*. 2018;74:23–31.
14. Ren L, Yan X, Zhou J, Tong J, Su X. Influence of chitosan concentration on mechanical and barrier properties of corn starch/chitosan films. *Int J Biol Macromol*. 2017;105:1636–1643.
15. Ravi Kumar MNV. A review of chitin and chitosan applications. *React Func Polym*. 2000;46:1–27.
16. Roberts GAF. Preparation of chitin and chitosan. In: Roberts GAF, ed. *Chitin Chemistry*. London, England: Macmillan Education; 1992:54–84.
17. Dutta PK, Dutta J, Tripathi V. Chitin and chitosan: chemistry, properties and applications. *J Sci Ind Res*. 2004;63:20–31.
18. Arshadi M, Faraji AR, Mehravar M. Dye removal from aqueous solution by cobalt-nano particles decorated aluminum silicate: kinetic, thermodynamic and mechanism studies. *J Colloid Interface Sci*. 2015;440:91–101.
19. Kyzas G, Bikiaris D. Recent modifications of chitosan for adsorption applications: a critical and systematic review *Marine Drugs*. 2015;13:312–337.
20. Khan SB, Ali F, Kamal T, Anwar Y, Asiri AM, Seo J. CuO embedded chitosan spheres as antibacterial adsorbent for dyes. *Int J Biol Macromolec*. 2016;88:113–119.
21. Zhu L, Cao L, Su G, et al. Effect of post heat treatment on microstructure and photocatalytic activities of TiO2 nanoribbons. *Appl Surf Sci*. 2011;257:7932–7937.
22. Ganguly P, Byrne C, Breen A, Pillai SC. Antimicrobial activity of photocatalysts: fundamentals, mechanisms, kinetics and recent advances. *Appl Catalysis B*. 2018;225:51–75.
23. Kołodziejczak-Radzimska A, Jesionowski T. Zinc oxide – from synthesis to application: a review. *Materials*. 2014;7:2833–2881.
24. Segets D, Gradl J, Taylor RK, Vassilev V, Peukert W. Analysis of optical absorbance spectra for the determination of ZnO nanoparticle size distribution, solubility, and surface energy. *ACS Nano*. 2009;3:1703–1710.
25. Sarkheil M, Johari SA, et al. Acute toxicity, uptake, and elimination of zinc oxide nanoparticles (ZnO NPs) using saltwater microcrustacean, *Artemia franciscana*. *Environ Toxicol Pharmacol*. 2018;57:181–188.
26. Tian C, Zhang Q, Wu A, et al. Cost-effective large-scale synthesis of ZnO photocatalyst with excellent performance for dye photodegradation. *Chem Commun*. 2012;48:2858–2860.
27. Xie J, Wang H, Duan M, Zhang L. Synthesis and photocatalysis properties of ZnO structures with different morphologies via hydrothermal method. *Appl Surf Sci*. 2011;257:6358–6363.
28. He L, Tong Z, Wang Z, et al. Effects of calcination temperature and heating rate on the photocatalytic properties of ZnO prepared by pyrolysis. *J Colloid Interface Sci*. 2018;509:448–456.
29. Ong CB, Ng LY, Mohammad AW. A review of ZnO nanoparticles as solar photocatalysts: synthesis, mechanisms and applications. *Renewable Sust Energy Rev*. 2018;81:536–551.
30. Ma X, Zhang B, Cong Q, et al. Organic/inorganic nanocomposites of ZnO/CuO/chitosan with improved properties. *Mater Chem Phys*. 2016;178:88–97.
31. Tang J, Durrant JR, Klug DR. Mechanism of photocatalytic water splitting in TiO2: reaction of water with photoholes, importance of charge carrier dynamics, and evidence for four-hole chemistry. *J Am Chem Soc*. 2008;130:13885–13891.
32. Liu Z-L, Deng J-C, Deng J-J, Li F-F. Fabrication and photocatalysis of CuO/ZnO nano-composites via a new method. *Mater Sci Eng B*. 2008;150:99–104.
33. Moretti G, Fierro G, Lo Jacono M, Porta P. Characterization of CuO–ZnO catalysts by X- ray photoelectron spectroscopy: precursors, calcined and reduced samples. *Surface Interface Anal*. 1989;14:325–336.
34. Sheini FJ, Singh J, Srivasatva O, Joag DS, More MA. Electrochemical synthesis of Cu/ZnO nanocomposite films and their efficient field emission behaviour. *Appl Surface Sci*. 2010;256:2110–2114.
35. Hassanzadeh-Tabrizi SA, Motlagh MM, Salahshour S. Synthesis of ZnO/CuO nanocomposite immobilized on γ-Al2O3 and application for removal of methyl orange. *Appl Surface Sci*. 2016;384:237–243.
36. Katoch A, Choi S-W, Kim J-H, Lee JH, Lee J-S, Kim SS. Importance of the nanograin size on the H2S-sensing properties of ZnO–CuO composite nanofibers. *Sens Actuat B Chem*. 2015;214:111–116.
37. Batra N, Tomar M, Gupta V. ZnO–CuO composite matrix based reagentless biosensor for detection of total cholesterol. *Biosens Bioelect*. 2015;67:263–271.
38. Mateos-Pedrero C, Silva H, Tanaka PDA, et al. CuO/ZnO catalysts for methanol steam reforming: the role of the support polarity ratio and surface area. *Appl Catalys B Environ*. 2015;174–175:67-76.
39. Soejima T, Takada K, Ito S. Alkaline vapor oxidation synthesis and electrocatalytic activity toward glucose oxidation of CuO/ZnO composite nanoarrays. *Appl Surface Sci*. 2013;277:192–200.
40. Harish S, Archana J, Sabarinathan M, et al. Controlled structural and compositional characteristic of visible light active ZnO/CuO photocatalyst for the degradation of organic pollutant. *Appl Surface Sci*. 2017;418:103–112.
41. Wu F, Wang X, Hu S, et al. Solid-state preparation of CuO/ZnO nanocomposites for functional supercapacitor electrodes and photocatalysts with enhanced photocatalytic properties. *Int J Hydrogen Energy*. 2017;42:30098–30108.
42. Sathishkumar P, Sweena R, Wu JJ, Anandan S. Synthesis of CuO-ZnO nanophotocatalyst for visible light assisted degradation of a textile dye in aqueous solution. *Chem Eng J*. 2011;171:136–140.
43. Sharfalddin A, Alzahrani E, Alamoudi M. Micro, sono, photocatalytic degradation of eosin B using ferric oxide doped with cobalt. *Am Chem Sci J*. 2016;13:1–13.
44. Sharfalddin A, Alzahrani E, Alamoudi M. Investigation of the synergism of hybrid advanced oxidation processes with an oxidation agent to degrade three dyes. *Res Chem Intermed*. 2016;43:1–15.
45. Salehi M, Hashemipour H, Mirzaee M. Experimental study of influencing factors and kinetics in catalytic removal of methylene blue with TiO2 nanopowder. *Am J Environ Eng*. 2012;2:1–7.
46. Jassal V, Shanker U, Kaith B. *Aegle marmelos* mediated green synthesis of different nanostructured metal hexacyanoferrates: activity against photodegradation of harmful organic dyes. *Scientifica*. 2016;2016:2715026.
47. Chaudhari P, Chaudhari V, Mishra S. Low temperature synthesis of mixed phase titania nanoparticles with high yield, its mechanism and enhanced photoactivity. *Mater Res*. 2016;19:446–450.
48. Hadjltaief HB, Ameur SB, Da Costa P, Zina MB, Galvez ME. Photocatalytic decolorization of cationic and anionic dyes over ZnO nanoparticle immobilized on natural Tunisian clay. *Appl Clay Sci*. 2018;152:148–157.
49. Madeleine-Perdrillat C, Karbowiak T, Debeaufort F, et al. Effect of hydration on molecular dynamics and structure in chitosan films. *Food Hydrocol*. 2016;61:57–65.

50. Azad AK, Sermsintham N, Chandrkrachang S, Stevens WF. Chitosan membrane as a wound-healing dressing: characterization and clinical application. *J Biomed Mater Res B Appl Biomater*. 2004;69:216–222.
51. Averineni RK, Sunderajan SG, Mutalik S, et al. Development of mucoadhesive buccal films for the treatment of oral sub-mucous fibrosis: a preliminary study. *Pharmaceut Dev Tech*. 2009;14:199–207.
52. Qi L, Xu Z, Jiang X, Hu C, Zou X. Preparation and antibacterial activity of chitosan nanoparticles. *Carbohydr Res*. 2004;339:2693–2700.
53. Pang X, Zhitomirsky I. Electrodeposition of composite hydroxyapatite–chitosan films. *Mater Chem Phys*. 2005;94:245–251.
54. Fernández-de Castro L, Mengíbar M, Arroyo ÁLS, Villarán MC, Díaz de Apodaca E, Heras Á. Films of chitosan and chitosan-oligosaccharide neutralized and thermally treated: effects on its antibacterial and other activities. *LWT-Food Sci Technol*. 2016;73:368–374.
55. Rubilar JF, Candia D, Cobos A, Díaz O, Pedreschi F. Effect of nanoclay and ethyl-Nα-dodecanoyl-l-arginate hydrochloride (LAE) on physico-mechanical properties of chitosan films. *LWT-Food Sci Technol*. 2016;72:206–214.
56. Lei H, Nie R-F, Fei J-H, Hou Z-Y. Preparation of Cu/ZnO/Al2O3 catalysts in a solvent-free routine for CO hydrogenation. *J Zhejiang Univ Sci A*. 2012;13:395–406.
57. Habibi MH, Karimi B. Preparation of nanostructure CuO/ZnO mixed oxide by sol–gel thermal decomposition of a CuCO3 and ZnCO3: TG, DTG, XRD, FESEM and DRS investigations. *J Ind Eng Chem*. 2014;20:925–929.
58. Saravanan R, Karthikeyan S, Gupta VK, et al. Enhanced photocatalytic activity of ZnO/CuO nanocomposite for the degradation of textile dye on visible light illumination. *Mater Sci Eng C*. 2013;33:91–98.
59. Arzate-Vázquez I, Chanona-Pérez JJ, Calderón-Domínguez G, et al. Microstructural characterization of chitosan and alginate films by microscopy techniques and texture image analysis. *Carbohydr Polym*. 2012;87:289–299.
60. Jiang R, Zhu H, Li X, Xiao L. Visible light photocatalytic decolourization of C.I. Acid Red 66 by chitosan capped CdS composite nanoparticles. *Chem Eng J*. 2009;152:537–542.
61. Foe K, Boland P, Namkoong G, Gu D, Baumgart H, Abdel-Fattah TM. Self-organized crystal growth of nanostructured ZnO morphologies by hydrothermal synthesis. *ECS Trans*. 2010;25:3–7.
62. Katayama H, Banba N, Sugimura Y, et al. Subcellular compartmentation of strontium and zinc in mulberry idioblasts in relation to phytoremediation potential. *Environ Exp Bot*. 2013;85:30–35.
63. Shinto H, Aso Y, Fukasawa T, Higashitani K. Adhesion of melanoma cells to the surfaces of microspheres studied by atomic force microscopy. *Colloids Surf B Biointerfaces*. 2012;91:114–121.
64. Yang H, Wang Y, Lai S, et al. Application of atomic force microscopy as a nanotechnology tool in food science. *J Food Sci*. 2007;72:R65–R75.
65. Ploehn HJ, Liu C. Quantitative analysis of montmorillonite platelet size by atomic force microscopy. *Ind Eng Chem Res*. 2006;45:7025–7034.
66. Basri H, Irfan M, Irfan M, Lau WJ, Kartohardjono S. Quantitative analysis of MWCNT agglomeration in polymeric-based membranes using atomic force microscope. *Surf Interface Anal*. 2017;49:55–62.
67. Chowdhury PR, Bhattacharyya KG. Ni/Ti layered double hydroxide: synthesis, characterization and application as a photocatalyst for visible light degradation of aqueous methylene blue. *Dalton Trans*. 2015;44:6809–6824.
68. Tian J, Leng Y, Zhao Z, et al. Carbon quantum dots/hydrogenated TiO2 nanobelt heterostructures and their broad spectrum photocatalytic properties under UV, visible, and near-infrared irradiation. *Nano Energy*. 2015;11:419–427.
69. Lin J, Shen J, Wang R, et al. Nano-p–n junctions on surface-coarsened TiO2 nanobelts with enhanced photocatalytic activity. *J Mater Chem*. 2011;21:5106–5113.
70. Dai K, Dawson G, Yang S, Chen Z, Lu L. Large scale preparing carbon nanotube/zinc oxide hybrid and its application for highly reusable photocatalyst. *Chem Eng J*. 2012;191:571–578.
71. Kumar A, Paliwal M, Ameta R, Ameta S. Oxidation of fast green FCF by the solar photo-Fenton process. *J Iranian Chem Soc*. 2008;5:346–351.
72. Carneiro PA, Nogueira RFP, Zanoni MVB. Homogeneous photodegradation of C.I. Reactive Blue 4 using a photo-Fenton process under artificial and solar irradiation. *Dyes Pigments*. 2007;74:127–132.
73. Anku WW, Oppong SO-B, Shukla SK, Agorku ES, Govender PP. Cobalt doped ZrO2 decorated multiwalled carbon nanotube: a promising nanocatalyst for photodegradation of indigo carmine and eosin Y dyes. *Prog Nat Sci Mater Int*. 2016;26:354–361.
74. Pourahmad A. Ag2S nanoparticle encapsulated in mesoporous material nanoparticles and its application for photocatalytic degradation of dye in aqueous solution. *Superlatt Microstruct*. 2012;52:276–287.
75. Lide DR. *CRC Handbook of Chemistry and Physics* (vol. 85). Boca Raton, FL: CRC Press; 2004.
76. Bessekhouad Y, Robert D, Weber J. Bi_2S3/TiO2 and CdS/TiO2 heterojunctions as an available configuration for photocatalytic degradation of organic pollutant. *J Photochem Photobiol A Chem*. 2004;163:569–580.
77. Zheng A, Fan Z, Li B, Shao Y, Liu J, Xi Y. Floatable photocatalysts of TiO2 nanofibers supported on hollow glass beads from fly ash for decomposing organic pollutants. *Nano Rep*. 2015;1:24–28.
78. Song S, Xu L, He Z, et al. Photocatalytic degradation of C.I. Direct Red 23 in aqueous solutions under UV irradiation using SrTiO3/CeO2 composite as the catalyst. *J Hazard Mater*. 2008;152:1301–1308.
79. Singh P, Mondal K, Sharma A. Reusable electrospun mesoporous ZnO nanofiber mats for photocatalytic degradation of polycyclic aromatic hydrocarbon dyes in wastewater. *J Colloid Interface Sci*. 2013;394:208–215.
80. Filice S, D'Angelo D, Libertino S, et al. Graphene oxide and titania hybrid Nafion membranes for efficient removal of methyl orange dye from water. *Carbon*. 2015;82:489–499.
81. Chong MN, Cho YJ, Poh PE, Jin B. Evaluation of titanium dioxide photocatalytic technology for the treatment of reactive Black 5 dye in synthetic and real greywater effluents. *J Clean Prod*. 2015;89:196–202.
82. Trabelsi H, Atheba GP, Hentati O, et al. Solar photocatalytic decolorization and degradation of methyl orange using supported TiO2. *J Adv Oxidat Technol*. 2016;19:79–84.